JOURNAL OF THEORETICAL AND APPLIED MECHANICS
45, 3, pp. 569-586, Warsaw 2007

EXPERIMENTAL INVESTIGATIONS OF JET FLOWS

Elżbieta Fornalik
Janusz S. Szmyd

AGH, University of Science and Technology, Faculty of Non-Ferrous Metals, Poland
e-mail: elaf@agh.edu.pl

The paper describes two kinds of jet flows: the confined and impinging jet flow. A triaxial thermoanemometer probe with a temperature sensor was used to study the confined jet flow. The time-average analysis of data resulted in a turbulence characteristic. It allowed the estimation of the budget of turbulent heat flux. The impinging jet flow was investigated by the Particle Image Velocimetry (PIV) method together with heat transfer analysis done with a liquid crystal film.

Key words: confined jet, impinging jet, turbulent heat flux, PIV

1. Introduction

In the industry, there are many kinds of jet flows which are mainly turbulent. Investigations of such flows in the industrial scale are very difficult. Therefore, experiments are done in laboratories with applications of various methods.

The confined jet flows can be found in ejectors, combustors, jet pumps and other devices, in which mixing layers of different mean velocities appear (Razinsky and Brighton, 1971). That kind of jet flows was studied by many researchers. It would be impossible to list all of them, however some of them have to be mentioned. Craya and Curtet (1955) described theory of the mixing zone of streams. Curtet (1958) introduced a similarity criterion to the appearance of recirculation. Becker *et al.* (1962) named this parameter as the Craya-Curtet number and investigated its influence on the flow structure. An experimental analysis of the confined jet was done by Barchilion and Curtet (1964), Brighton and Jones (1964). Champagne and Wygnanski (1971) investigated the turbulence characteristic for various conditions. Their work was continued by Razinsky and Brighton (1971). Non-isothermal flows were studied by Frota and Moffat (1982), Heist and Castro (1998), Keffer *et al.* (1977), Chevery and Tutu (1978), Suzuki *et al.* (1987), Kang and Suzuki (1982) and

Kang *et al.* (1979). The confined jest was investigated under various conditions with various experimental methods.

The impinging jet has a wide range of industrial applications in processes involving heating, cooling and drying. Advantages of impinging jets come from the effective removal of heat flux and easy adjustment to locations where it is necessary. The turbine cooling system consists of the jet array. The streams coming from the upstream-positioned jets merge, producing the crossflow. Many researchers, including Metzger and Korstad (1972), Bouchez and Goldstein (1975), Sparrow *et al.* (1975), Saad *et al.* (1980), Goldstein and Franchett (1988) and Huang *et al.* (1996) studied various aspects of the jet impingement heat transfer under the influence of the crossflow.

A triaxial thermoanemometer probe with a temperature wire was used to study the confined jet, whereas in the case of the impinging jet the Particle Image Velocimetry (PIV) accompanied by liquid crystal temperature measurements.

2. Confined jet

The name "confined jet" describes two streams of a fluid: primary circular stream entraining and mixing with the secondary annular stream in a confined chamber. If the ratio of velocities is large enough, the recirculation zone may appear. In the presented study, special attention is paid to the budget of turbulent heat transfer.

2.1. Experimental apparatus

A schematic diagram of the experimental apparatus is shown in Fig. 1. The set-up has been located at the laboratory of the Institute of Thermal Machinery at the Technical University of Częstochowa. The air is drawn from atmosphere through air filter (1) by blower (2). The pure and regulated air stream is divided in two in air divider (4); i.e. into the primary circular stream and the secondary annular stream. The air of the primary stream is heated by electrical heater (6). The temperature difference between the circular and annular streams is 20 K. The regulated and heated air stream is then discharged from aluminium inner nozzle (11) with diameter $d = 0.040\,\mathrm{m}$. The nozzle is designed to obtain coaxial streams (the circular primary stream and the annular secondary stream) at the inlet of the test section. Fine mesh screens (8) and honeycomb (9) are used to condition the secondary stream. The size of the measuring section (plexi-glass tube) is: diameter $D = 0.192\,\mathrm{m}$, length

$l = 2\,\mathrm{m}$. The mean velocity of the primary air stream equals $\overline{U}_1 = 20\,\mathrm{m/s}$ and the mean velocity of secondary stream is $\overline{U}_2 = 1\,\mathrm{m/s}$.

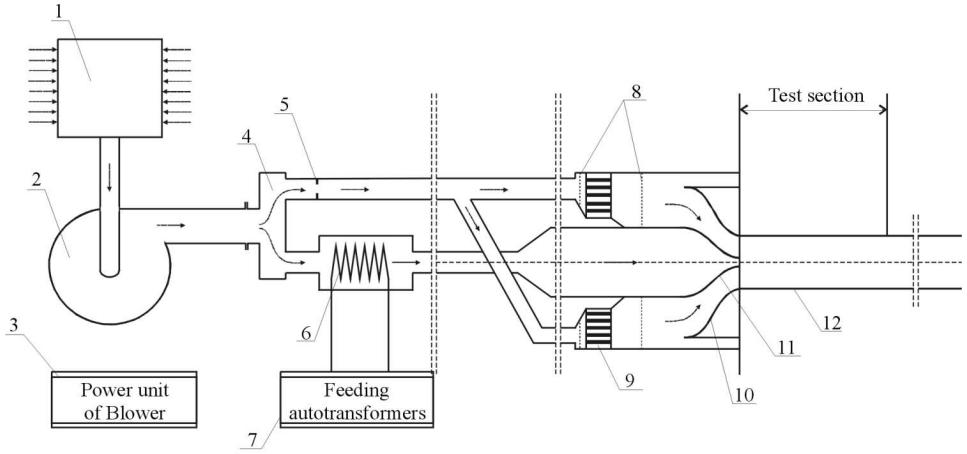

Fig. 1. A schematic diagram of the experimental set-up in the case of confined jet; 1 – air filter, 2 – blower, 3 – thyristor system, 4 – air divider, 5 – orifice, 6 – electric heater, 7 – autotransformers, 8 – fine mesh screen, 9 – honeycomb, 10 – outer nozzle, 11 – inner nozzle, 12 – test section

2.2. Procedure

Geometry and initial conditions were determined by the similarity criterion: i.e. the Craya-Curtet number which expresses the influence of the input momentum flux distribution on the confined jet system. The Craya-Curtet number is defined by

$$\begin{aligned} \mathrm{Ct} &= \frac{U_m}{U^*} \\ U^* &= \sqrt{(\overline{U}_1^2 - \overline{U}_2^2)b^2 + \frac{1}{2}(\overline{U}_2^2 - U_m^2)} \\ U_m &= (\overline{U}_1 - \overline{U}_2)b^2 + \overline{U}_2 \end{aligned} \tag{2.1}$$

The Craya-Curtet number was set up to be $\mathrm{Ct} = 0.5$, for which the recirculation zone was large enough for the investigations. The location of the recirculation zone was preliminary monitored by a hot-wire probe with two parallel tungsten filaments.

The test section was divided into 17 cross sections and in each cross-section 23 measurement points were situated. The measurements were done by the DANTEC hot-wire anemometry system with four channels, one of which was for temperature and the other three for velocity components. It allowed simultaneous measurements of velocity and temperature. The sampling rate was

20 kHz per channel. The sampled raw data were stored for further analysis to obtain the mean velocity components, Reynolds normal and shear stresses, temperature and its fluctuation and turbulent heat flux components. The technique of estimation of all the above mentioned quantities is precisely described in Fornalik *et al.* (1998).

2.3. Results

The non-dimensional value of the velocity component was set up as the ordinate axis in Fig. 2. There can be recognised an internal, circular stream of a high velocity $(0 \leqslant r/d \leqslant 0.6)$ and an external, annular stream of a low velocity $(0.6 \leqslant r/d \leqslant 2.1)$. In the first cross-section $(x/d = 1)$ the primary-stream potential core can be observed, but it quickly disappears. The most important information, which could be read from Fig. 3, is related to formation of the recirculation zone. The negative values of velocity appear in the vicinity of the wall on the 4th cross-section $(x/d = 4)$, and going downstream successively, the reverse flow is developing. The measured recirculation zone is a little larger than 0.68 m $x/d = 17$ (beyond the investigated zone), therefore it is not possible to specify the reattachment point.

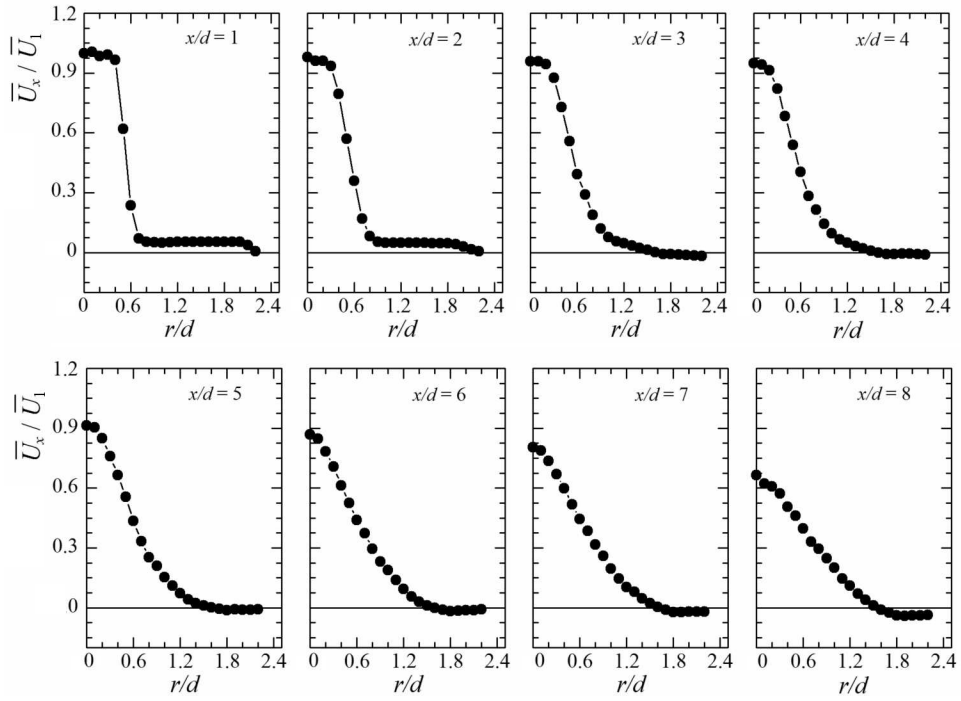

Fig. 2. Distribution of the longitudinal velocity component

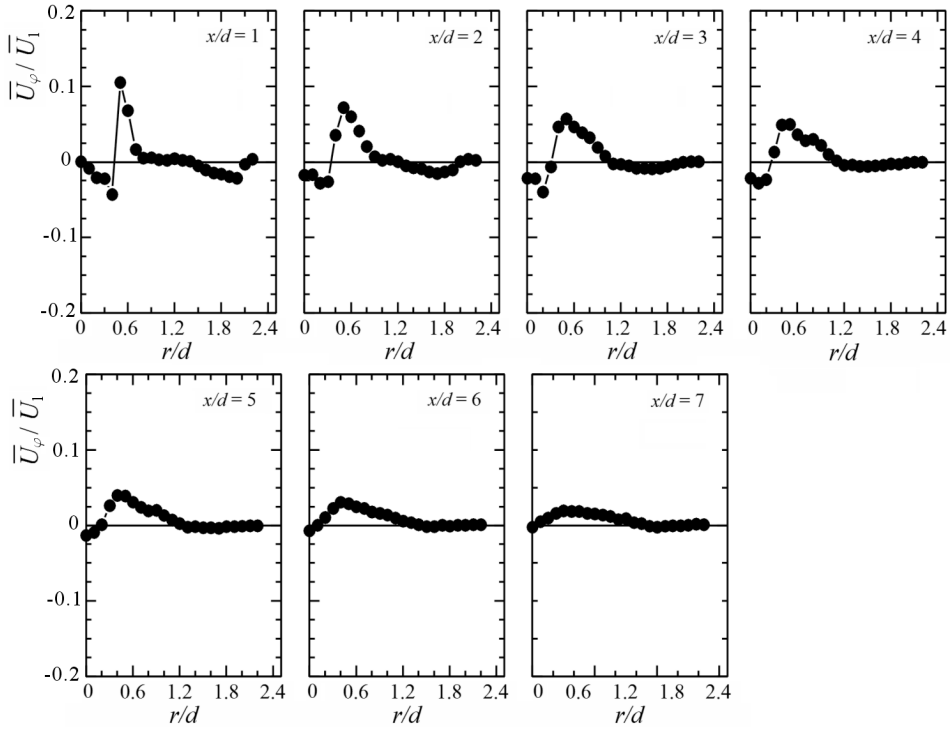

Fig. 3. Distribution of the angular velocity component

The flow was assumed to be two-dimensional (symmetrical), but the primary stream was slightly twisted in a few first measured profiles. The third angular component of the velocity vector $\overline{U}_\varphi$ appeared and it affected all measured quantities. The distribution of its non-dimensional value is presented in Fig. 3. In magnitude, it is much smaller than the other two components of the velocity vector. However, in the first four cross-sections, a change of the direction can be observed. In the first cross-section $(x/d = 1)$, the circular stream is twisted, which is suggested by the change in the sign of the value in the range of r/d from 0 to about 0.6. The value of the velocity for the angular stream changes its sign in the range of r/d from 1.2 to about 2.2, which also suggests twist of the stream. Going downstream, the magnitude of the third velocity component becomes smaller, and from the fifth cross-section $(x/d = 5)$ only the circular stream is disturbed.

The data related to the distribution of temperature, Reynolds normal and shear stresses and also to turbulent heat flux components were presented in Fornalik and Szmyd (2005). The problem of heat transfer budget will be discussed in detail in this paper.

The governing equations are presented below (Eqs. $(2.2)_{1,2,3}$) in the cylindrical co-ordinate system (suitable for examined geometry). They are expressed in four groups representing (1) convection, (2) production due to mean velocity and mean temperature fields, (3) diffusion and (4) transfer due to pressure correlation, molecular transfer due to viscosity and thermal conductance of the fluid. The last (fourth) term is taken as a closure term, because the pressure-temperature correlations cannot be measured and the molecular transport of turbulent heat flux is impossible to obtain. The closure term is identified with the pressure-temperature correlation (the molecular transport due to viscosity and thermal conductance can be neglected, because of low influence on the budget), Kasagi (1991)

$$
\begin{aligned}
&\underbrace{\overline{U}_x\frac{\partial\overline{u_x\theta}}{\partial x}+\overline{U}_r\frac{\partial\overline{u_x\theta}}{\partial r}}_{(1)}=\underbrace{-\overline{u_x\theta}\frac{\partial\overline{U}_x}{\partial x}-\overline{u_r\theta}\frac{\partial\overline{U}_r}{\partial r}-\overline{u_xu_x}\frac{\partial\overline{T}}{\partial x}-\overline{u_xu_r}\frac{\partial\overline{T}}{\partial r}}_{(2)}+\\
&\underbrace{-\frac{\partial}{\partial x}(\overline{u_xu_x\theta})-\frac{1}{r}\frac{\partial}{\partial r}(r\overline{u_xu_r\theta})}_{(3)}+\\
&\underbrace{-\frac{1}{\rho}\theta\overline{\frac{\partial p}{\partial x}}+\nu\Big(\overline{\theta\frac{\partial^2u_x}{\partial x^2}}+\overline{\theta\frac{\partial^2u_x}{\partial r^2}}+\frac{1}{r}\overline{\theta\frac{\partial u_x}{\partial r}}\Big)+a\Big(\overline{u_x\frac{\partial^2\theta}{\partial x^2}}+\overline{u_x\frac{\partial^2\theta}{\partial r^2}}+\frac{1}{r}\overline{u_x\frac{\partial\theta}{\partial r}}\Big)}_{(4)}\\
&\underbrace{\overline{U}_x\frac{\partial\overline{u_r\theta}}{\partial x}+\overline{U}_r\frac{\partial\overline{u_r\theta}}{\partial r}}_{(1)}=\underbrace{-\overline{u_x\theta}\frac{\partial\overline{U}_r}{\partial x}-\overline{u_r\theta}\frac{\partial\overline{U}_r}{\partial r}-\overline{u_xu_r}\frac{\partial\overline{T}}{\partial x}-\overline{u_ru_r}\frac{\partial\overline{T}}{\partial r}}_{(2)}+\\
&\underbrace{-\frac{\partial}{\partial x}(\overline{u_xu_r\theta})-\frac{1}{r}\frac{\partial}{\partial r}(r\overline{u_ru_r\theta})+\frac{1}{r}(\overline{u_\varphi u_\varphi\theta})+\frac{2}{r}\overline{U}_\varphi\overline{u_\varphi\theta}}_{(3)}+\qquad(2.2)\\
&\underbrace{-\frac{1}{\rho}\theta\overline{\frac{\partial p}{\partial r}}+\nu\Big(\overline{\theta\frac{\partial^2u_r}{\partial x^2}}+\overline{\theta\frac{\partial^2u_r}{\partial r^2}}+\frac{1}{r}\overline{\theta\frac{\partial u_r}{\partial r}}-\frac{1}{r^2}\overline{u_r\theta}\Big)+a\Big(\overline{u_r\frac{\partial^2\theta}{\partial x^2}}+\overline{u_r\frac{\partial^2\theta}{\partial r^2}}+\frac{1}{r}\overline{u_r\frac{\partial\theta}{\partial r}}\Big)}_{(4)}\\
&\underbrace{\overline{U}_x\frac{\partial\overline{u_\varphi\theta}}{\partial x}+\overline{U}_r\frac{\partial\overline{u_\varphi\theta}}{\partial r}}_{(1)}=\underbrace{-\overline{u_x\theta}\frac{\partial\overline{U}_\varphi}{\partial x}-\overline{u_r\theta}\frac{\partial\overline{U}_\varphi}{\partial r}-\overline{u_xu_\varphi}\frac{\partial\overline{T}}{\partial x}-\overline{u_ru_\varphi}\frac{\partial\overline{T}}{\partial r}}_{(2)}+\\
&\underbrace{-\frac{\partial}{\partial x}(\overline{u_xu_\varphi\theta})-\frac{\partial}{\partial r}(\overline{u_ru_\varphi\theta})-\frac{2}{r}(\overline{u_ru_\varphi\theta})-\frac{1}{r}\overline{U}_r\overline{u_\varphi\theta}-\frac{1}{r}\overline{U}_\varphi\overline{u_r\theta}}_{(3)}+\\
&\underbrace{+\nu\Big(\overline{\theta\frac{\partial^2u_\varphi}{\partial x^2}}+\overline{\theta\frac{\partial^2u_\varphi}{\partial r^2}}+\frac{1}{r}\overline{\theta\frac{\partial u_\varphi}{\partial r}}-\frac{1}{r^2}\overline{u_\varphi\theta}\Big)+a\Big(\overline{u_\varphi\frac{\partial^2\theta}{\partial x^2}}+\overline{u_\varphi\frac{\partial^2\theta}{\partial r^2}}+\frac{1}{r}\overline{u_\varphi\frac{\partial\theta}{\partial r}}\Big)}_{(4)}
\end{aligned}
$$

In Figs. 4-6, the budgets of particular components of turbulent heat flux are presented. In Fig. 4, the distribution of the axial component is shown. A distance from the centre of the channel is set up as the abscissa, and as the ordinate – the loss or the gain for the budget. A positive value of the particular term (loss) means that the larger quantity of turbulent heat flux flows up from the control volume than comes in. A negative value (gain) describes the opposite situation. Every term is marked as a line of different type (look-up the legend). Two terms are visibly dominant: the production term and the pressure-temperature term, which almost compensate each other. The production term is a gain for the budget in contrast to the pressure-temperature term (loss). They are dominant in the case of each turbulent heat flux component, but they take the highest values for the radial component presented in Fig. 5. The most intensive heat transfer processes are observed in the shear region between streams ($r/d \approx 0.5$). In the first graph ($x/d = 2$, $r/d = 0$-0.1), it is found that all terms are equal to zero, which is characteristic for a potential core. This is the potential core of primary stream. The potential core of secondary stream disappears before the place at which the first cross-section is measured. In the second graph ($x/d = 3$), it is not observed – the potential core of primary stream vanishes due to mixing of the streams.

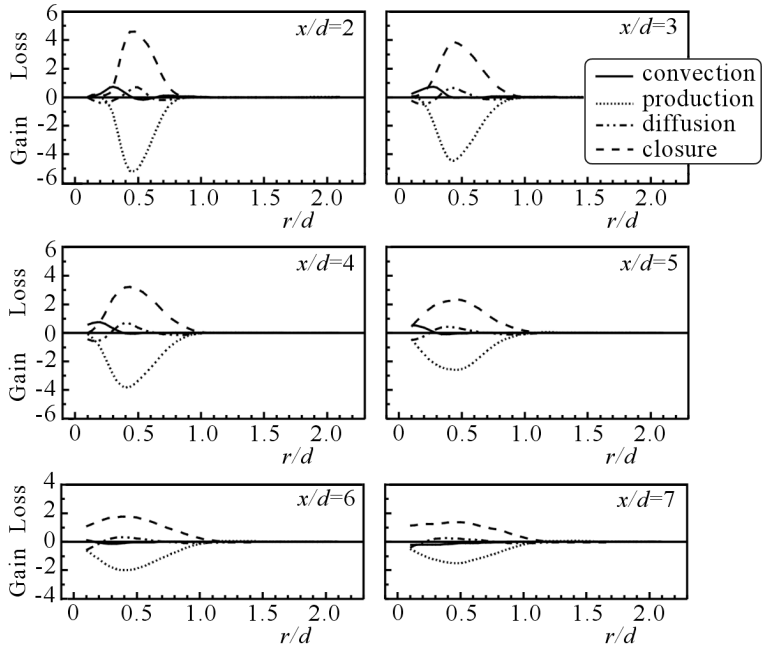

Fig. 4. Distribution of the budget for the axial component of turbulent heat flux in various cross-sections

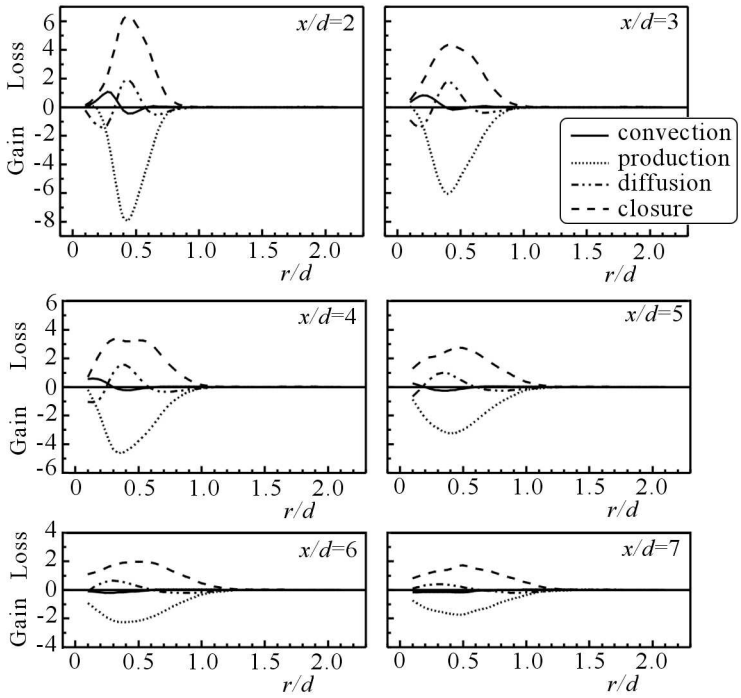

Fig. 5. Distribution of the budget for the radial component of turbulent heat flux in various cross-sections

It is worth to say that the distributions of diffusion and convection terms are very interesting. They are nearly complementary like the production and closure terms (but in a smaller scale). Near the centre of the channel ($r/d = 0.1$), the diffusion term makes a gain for the budget in contrast with the convection term. The opposite situation can be observed near the place of the most intensive streams mixing ($r/d = 0.5$), where the diffusion term takes positive values (loss) and the convection term takes negative values (gain). The diffusion transfers the heat from the mixing region of the jets (positive values – loss) toward the centre of the channel and walls, where it takes negative values (gain). The heat is transferred by convection from the circular stream (centre of the channel, $r/d = 0.1$), where it takes positive values (loss) to the secondary stream ($r/d > 0.5$), where its sign is negative (gain). Generally, it can be said that going downstream ($x/d = 5, 6, 7$), the heat transfer becomes less intensive, which does not depend on the way of transfer.

The distribution of the budget for the radial component of turbulent heat flux presented in Fig. 5 is very similar to the budget for the axial component. The only difference is in the magnitude of particular terms. The difference in the distribution of the budget can be observed in Fig. 6. It presents the angular component of turbulent heat flux. The magnitudes of all terms are much smaller than in the case of the axial and radial components.

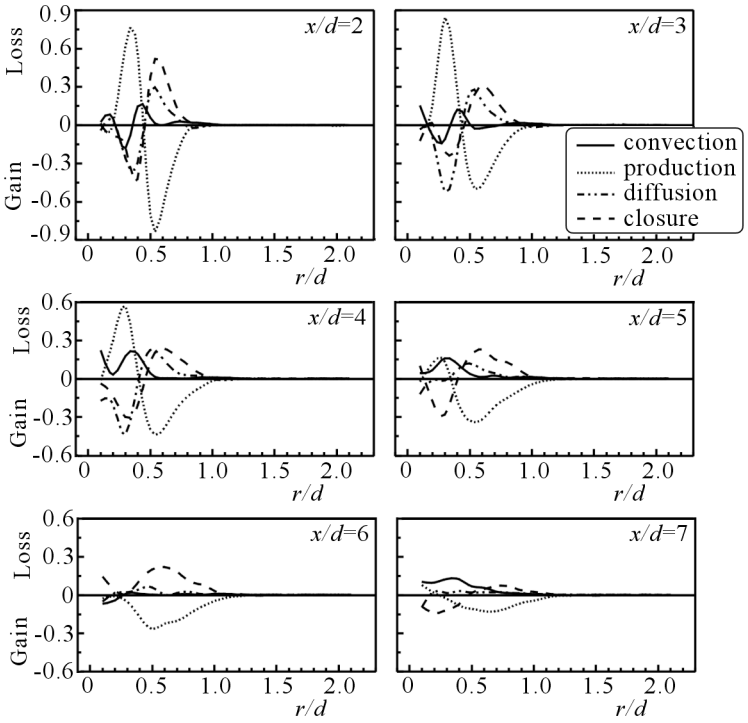

Fig. 6. Distribution of the budget for the angular component of turbulent heat flux in various cross-sections

The heat transfer from the circular stream toward the annular one is well visible. The region of intensive mixing between the streams ($r/d = 0.5$) can be easily identified, since it is the region where the heat transfer changes the direction. The production term is dominant, especially in the first three cross-sections (x/d = 2-4). Turbulent heat flux is transferred form the circular primary stream to the annular secondary stream. The diffusion and closure terms compensate the production term, what can be found for $x/d = 3$ and $x/d = 4$. The convection term has small influence on the heat flux transfer. It has some effect only for the circular stream causing heat flux transfer from its outer region to its central part. Going downstream, the heat transfer becomes less intensive.

2.4. Comments

The most important area for the heat transfer in the case of the confined jet with the recirculation zone appeared in the mixing region of circular and annular streams (the shear region). Two terms were dominant in the budget of turbulent heat flux: production term and pressure-temperature term. The heat transfer processes were the most intensive in the radial direction. The

angular component of the heat flux budget showed different tendency, but its magnitude was the smallest.

3. Impinging jets

3.1. Experimental apparatus

Figure 7 is a schematic illustration of the experimental apparatus used in the present study. Water used as the working fluid was driven by the head difference between constant-head upper tank (1) and an outlet gate of horizontally installed test section (4). The gate was made of an acrylic plate to enable optical access for flow visualizations. Two round impinging jet nozzles (9), with the diameter d of 6 mm, were mounted flush with the bottom wall of the test section. The main flow supplied into the test section through contraction (3) served as a crossflow for the impinging jets.

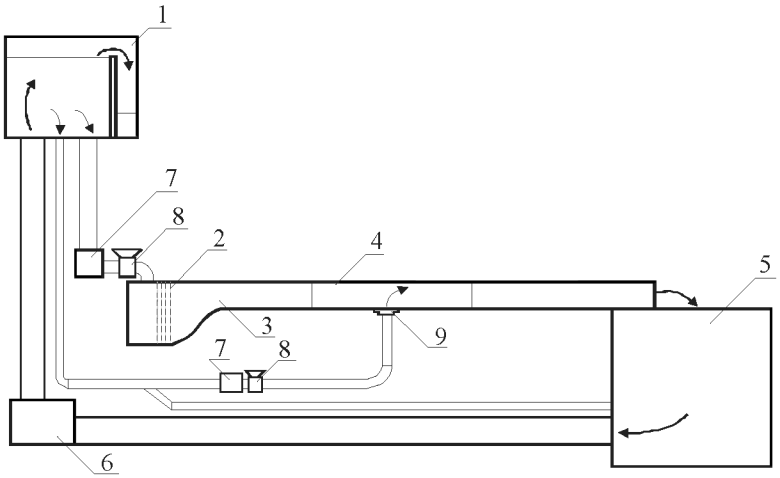

Fig. 7. A schematic diagram of the experimental set-up in the case of impinging jets; 1 – upper tank, 2 – wire gauge, 3 – contraction, 4 – test section, 5 – lower tank, 6 – pump, 7 – flow meters, 8 – valves, 9 – jet nozzles

Dimensions of the test section are shown in Fig. 8 together with geometrical parameters, jet nozzles arrangements and coordinate system set up in the present study. The test section was rectangular, 432 mm wide. The height of the test section, H_D, was 30 mm in the case of the jets normal to the target wall, and 21 mm to keep the same impinging distance in the case of oblique jets. The two jets were situated in an in-line arrangement with a streamwise distance of $10d$. The skew angels between the directions of the impinging jets

and the crossflow in the horizontal plane were set to be $+90°$ for the upstream-side jet, Jet 1, and $-90°$ for the downstream-side one, Jet 2, while the pitch angle measured up from the nozzle-installed wall was fixed at $45°$ for both jets. The pitch angles of both jets were changed to be $90°$ for the vertical impingement case.

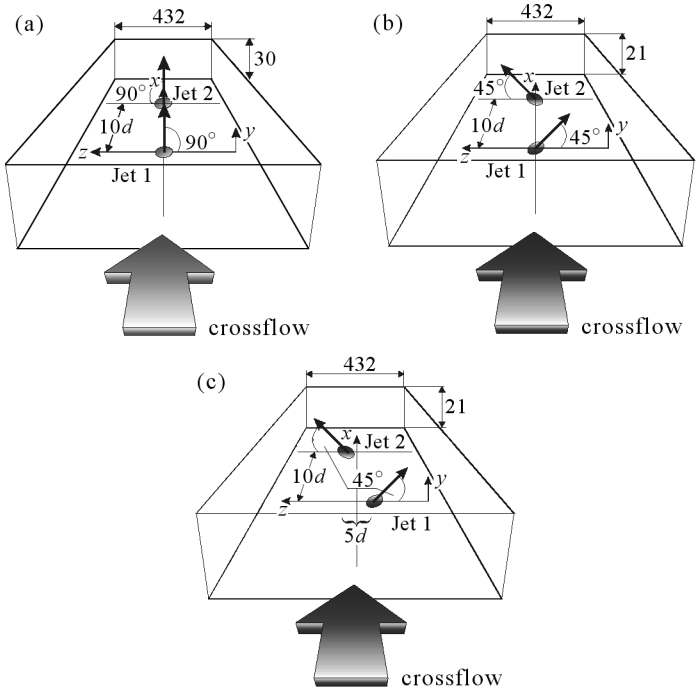

Fig. 8. Test section and twin jet nozzles; (a) vertical nozzles, (b) inclined nozzles, in-line arrangement, (c) inclined nozzles, staggered arrangement

3.2. Procedure

The Reynolds number of the crossflow, Re, based on the hydraulic diameter of the test section was set to be equal to 5 000. The velocity ratio of the jet to the crossflow, V_R, was set up to be 5. Local Nusselt number, Nu, based on the hydraulic diameter is defined as follows

$$\mathrm{Nu} = \frac{\alpha(2H_D)}{\lambda} \tag{3.1}$$

where α is the heat transfer coefficient calculated from Eq. (3.2)

$$\alpha = \frac{q_W}{T_W - T_0} \tag{3.2}$$

where λ is the thermal conductivity, T_W and T_0 are the local temperature of the target wall and the inlet flow temperature, respectively, q_W is the target wall heat flux calculated from the electric power input. The heat conduction loss towards the backside of the target wall was neglected since it was relatively small, approximately 3% of the total heat flux. The heat radiation loss from the surface of the target wall was also neglected.

The cross-sectional images of the flow patterns were taken through the acrylic plate with a CCD camera set up downstream. Velocity vectors were estimated with the PIV system from the scattering images of fine TiO_2 particles injected into the jet flows and illuminated by a planar Nd:YAG pulse laser light.

The temperature distribution of the heat transfer target surface was measured with thermochromic liquid crystal sheets attached to the back of the target surface. The images of the color liquid crystal surface were taken with another CCD camera installed above the test section. The colors of the images were transformed into the temperature distribution by the neural network technique described in Nakabe *et al.* (1998). Afterwards, the Nusselt number could be estimated.

3.3. Results

The velocity vector maps of twin vertical jets together with the distribution of the Nusselt number are shown in Fig. 9. The measured cross-section were at streamwise locations: (a) $x/d = 10$, (b) $x/d = 20$, (c) $x/d = 30$ and (d) $x/d = 40$. Two large longitudinal counter-rotating vortices are visible. Their positions correspond very well to the position of area of enhanced heat transfer presented in Fig. 9e. Values of the Nusselt number in the range from $z/d = -5$ to $z/d = 5$ are larger than outside this area.

The velocity vector maps of two inclined jets in the in-line arrangement together with the distribution of the Nusselt number are shown in Fig. 10. The measured cross-sections were at four streamwise locations: (a) $x/d = 10$, (b) $x/d = 20$, (c) $x/d = 30$ and (d) $x/d = 40$. The three large-scale longitudinal vortices plus one small-scale vortex can be recognized. These vortices can be observed even far downstream from the locations of the nozzles. It can be seen that the vortices forming each of the pairs are rotating in opposite directions, and that the areas of high spanwise velocity, close to the upper target wall, are related to the region of enhanced heat transfer, which is presented in Fig. 10e.

In Fig. 10e, the distribution of the Nusselt number at the same four locations as for the velocity vector maps are presented. The area of enhanced heat transfer is well visible. Two regions of high Nusselt numbers can be recognized.

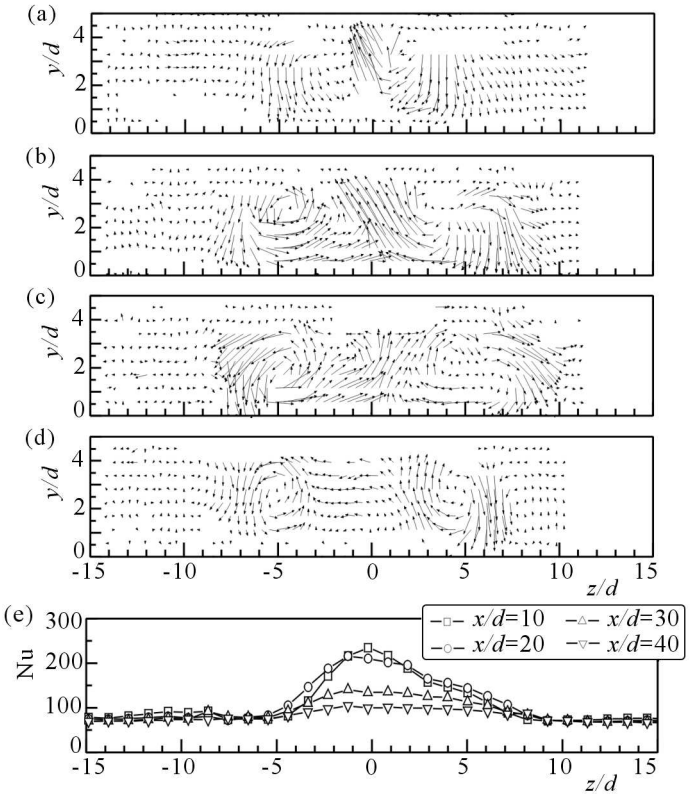

Fig. 9. Results for the twin vertical jets (Re = 5000, $V_R = 5$); (a)-(d) cross-sectional velocity vectors: (a) $x/d = 10$, (b) $x/d = 20$, (c) $x/d = 30$ and (d) $x/d = 40$, (e) distribution of the Nusselt number

The highest value of the Nusselt number is close to the location at $x/d = 10$ and $z/d = 4$, Nu = 250 value almost equal to the maximum value in the case of two vertical jets in Fig. 9e. The area of enhanced heat transfer becomes wider, however values of the Nusselt number are smaller. The comparison between the results of the velocity and Nusselt number measurements reveals a very good agreement between the vortex location and heat transfer enhancement region. The enhanced region is related to the paths of the large-scale longitudinal vortices.

The velocity vector maps of two inclined jets in the staggered arrangement together with the distribution of the Nusselt number are presented in Fig. 11. The measured cross-sections were at six locations: (a) $x/d = 0$, (b) $x/d = 5$, (c) $x/d = 10$, (d) $x/d = 20$, (e) $x/d = 30$ and (f) $x/d = 40$. The four vortices can be recognized. These longitudinal vortices form two pairs of counter-rotating vortices, which can be observed even far away from the locations of nozzles. The number of vortices is different from the case of the

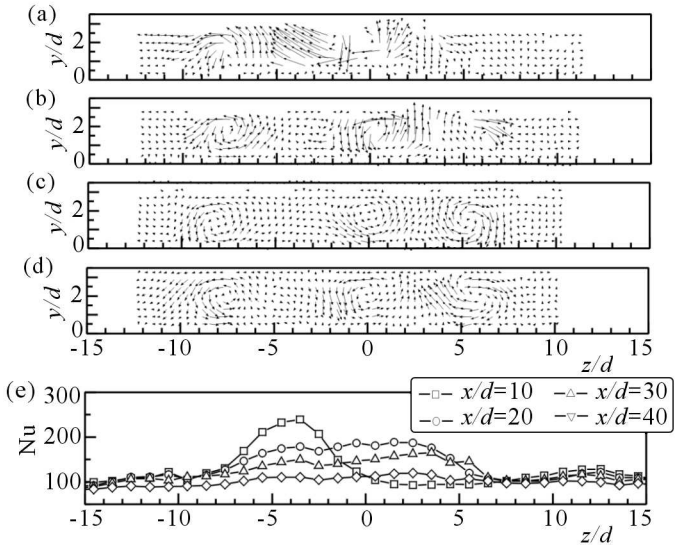

Fig. 10. Results for the twin inclined jets, in-line arrangement (Re = 5000, $V_R = 5$); (a)-(d) cross-sectional velocity vectors: (a) $x/d = 10$, (b) $x/d = 20$, (c) $x/d = 30$ and (d) $x/d = 40$, (e) distribution of the Nusselt number

in-line arrangement of the jets. The positions of vortices correspond very well to the region of enhanced heat transfer presented in Fig. 11e. The distribution of the Nusselt number presents two regions with maximum values, which are bigger more than twice than in the case of vertical jets and inclined jets in the in-line arrangement. The region of enhanced heat transfer elongates from $z/d = -10$ to $z/d = 10$ and is also wider than in the case of the in-line arrangement.

3.4. Comments

The large-scale longitudinal vortices are generated in the rectangular duct flow as the result of impinging jets. The number of vortices depends on the arrangement of the jet nozzles. For the vertical jets, two vortices are observed, for the inclined jets in the in-line arrangement three, while for the inclined jets in the staggered arrangement four ones are found. The path of the longitudinal vortices corresponds very well to the heat transfer enhancement regions for all kinds of arrangements of the jet nozzles. The interaction between the jets depending on the nozzles arrangements has serious influence on the vertical structure and the enhanced heat transfer regions as well.

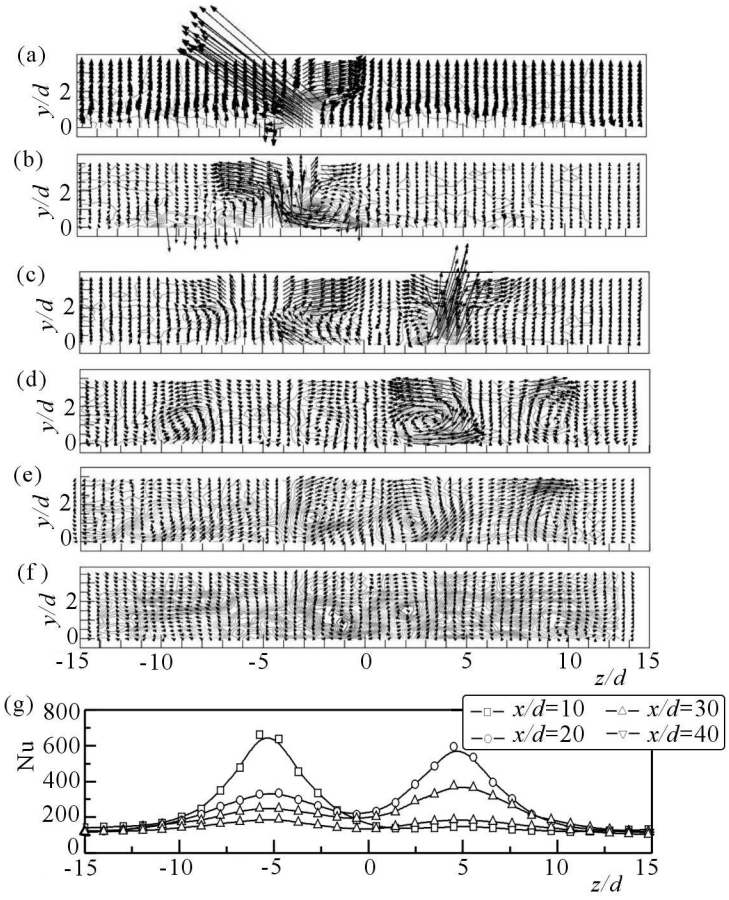

Fig. 11. Results for the twin inclined jets, staggered arrangement (Re = 5000, $V_R = 5$); (a)-(f) cross-sectional velocity vectors: (a) $x/d = 0$, (b) $x/d = 5$, (c) $x/d = 10$, (d) $x/d = 20$, (e) $x/d = 30$ and (f) $x/d = 40$, (e) distribution of Nusselt number

4. Conclusions

The experimental studies on two kinds of jet flows were presented. Various methods were applied: in the case of the confined jet a four-wire thermoanemometer probe was used, while in the case of impinging jets, the PIV and liquid crystal film technique was applied. The choice of the method depended on the character of the flow, fluid and investigated qualities. The results, analysis and comments were reported.

References

1. Barchilon M., Curtet R., 1964, Some details of the structure of an axisymmetric confined jet with backflow, *Trans. ASME: J. Basic Eng.*, **86**, 777-787

2. Becker H.A., Hottel H.C., Williams G.C., 1962, Mixing and flow in ducted turbulent streams, *Proceedings of the 9th Int. Symposium on Combustion, The Combustion Inst.*, Pittsburgh, 7-20

3. Bouchez J.P., Goldstein R.J., 1975, Impingement cooling from a circular jet in a cross flow, *Int. J. Heat and Mass Trans.*, **18**, 719-730

4. Brighton J.A., Jones J.B., 1964, Fully developed turbulent flow in annuli, *Trans. ASME: J. Basic Eng.*, **86**, 835-844

5. Champagne F.H., Wygnanski I.J., 1971, An experimental investigation of coaxial turbulent jets, *Int. J. Heat and Mass Trans.*, **14**, 1445-1464

6. Chevray R., Tutu N.K., 1978, Intermittency and preferential transport of heat in a round jet, *J. Fluid Mech.*, **88**, 133-160

7. Craya A., Curtet R., 1955, On the spreading of a confined jet, *Comptes-Rendus Acad. Sci.*, **241**, 621-622

8. Curtet R., 1958, Confined jets and recirculation phenomena with cold air, *Combustion and Flame*, **2**, 383-411

9. Fornalik E., Jaszczur M., Szmyd J.S., Klajny R., Nakabe K., Suzuki K., 1998, An application of a triaxial probe with temperature sensor to analysis of turbulent heat transfer in a confined coaxial jet, *Proceedings of the 4th KSME-JSME Fluids Engineering Conference*, Pusan, 513-516

10. Fornalik E., Szmyd J.S., 2005, Turbulent heat transfer in a confined jet, *Progress in Computational Fluid Dynamics*, **5**, 136-143

11. Frota M.N., Moffat R.J., 1982, Triple hot-wire technique for measurements of turbulence in heated flows, *Proceedings of the 7th Int. Heat Transfer Conference*, Monachium, 491-496

12. Goldstein R.J., Franchett M.E., 1988, Heat transfer from a flat surface to an oblique impinging jet, *Trans. ASME: J. Heat Transfer*, **110**, 84-90

13. Heist D.K., Castro I.P., 1998, Combined laser-doppler and cold wire anemometry for turbulent heat flux measurement, *Experimetns in Fluids*, **24**, 375-381

14. Huang Y., Ekkad S.V., Han J.C., 1996, Detailed heat transfer coefficient distributions under an array of inclined impinging jets using a transient liquid crystal technique, *Proceedings of the 9th Int. Symposium on Transport Phenomena in Thermal-Fluid Engineering*, Singapore, 807-812

15. KANG Y., SUZUKI K., 1982, Numerical study of wall heat transfer in the recirculating flow region of a confined jet, *Heat Transfer Japanese Research*, **11**, 1, 44-69

16. KANG Y., SUZUKI K., SATO T., 1979, Convective heat transfer in an axisymmetric confined jet, *Studies in Heat Transfer*, Edit. T.F. Irvine *et al.*, Hemisphere, 103-125

17. KASAGI N., 1991, Direct numerical simulation data bases: an effective tool in fundamental studies of turbulent heat transfer, *Proceedings of the Japan-U.S. Science Seminar on Computers in Heat Transfer Science*, Oiso

18. KEFFER J.F., OLSEN G.J., KAWALL J.G., 1977, Intermittency in a thermal mixing layer, *J. Fluid Mech.*, **79**, 595-607

19. METZGER D.E., KORSTAD R.J., 1972, Effects of crossflow on impingement heat transfer, *Trans. ASME: J. Eng. Power*, **94**, 35-42.

20. NAKABE K., HIGASHIO A., CHEN W., SUZUKI K., KIM J.H., 1988, An experimental study on the flow and heat transfer characteristics of longitudinal vortices induced by an inclined impinging jet into a crossflow, *Proceedings of the 11th Int. Heat Transfer Conference*, Kyongju, 439-444

21. RAZINSKY E., BRIGHTON J.A., 1971, Confined jet mixing for nonseparating conditions, *Transactions of the ASME J. Basic Eng.*, **93**, 333-349

22. SAAD N.R., MUJUMDAR A.S., MESSEH W.A., DOUGLAS W.J.M., 1980, Local heat transfer characteristics for staggered arrays of circular impinging jets with crossflow of spent air, *ASME Paper 80-TH-23*, 105-112

23. SPARROW E.M., GOLDSTEIN R.J., ROUF M.A., 1975, Effect of nozzle-surface separation distance on impingement heat transfer for a jet in a crossflow, *Trans. ASME: J. Heat Transfer*, **97**, 528-533

24. SUZUKI K., SUGA K., OSHIKAWA Y., 1987, LDV Measurement of turbulence and test of turbulence models in recirculating flow, *Proceedings of the 6th Symposium on Turbulent Shear Flows*, Toulouse, 15.4.1-15.4.6

Badania eksperymentalne przepływów strumieniowych

Streszczenie

Zaprezentowane zostały badania eksperymentalne dotyczące dwóch rodzajów przepływów strumieniowych: strugi pierścieniowej oraz strugi uderzającej. Czterowłóknowa sonda termoanemometryczna wykorzystana została w badaniach związanych ze strugą pierścieniową. Analiza danych pozwoliła na wyznaczenie wielkości charakteryzujących przepływ turbulentny, ze szczególnym uwzględnieniem bilansu turbulentnego strumienia ciepła. W badaniach strugi uderzającej pod działaniem przepływu

krzyżowego do wyznaczenia pola prędkości wykorzystano metodę PIV (ang. *Particle Image Velocimetry*). Badaniom przepływu towarzyszyła analiza wymiany ciepła przy użyciu termoczułych ciekłych kryształów w postaci cienkiego filmu. Zaobserwowane zostały wiry, które w głównej mierze odpowiadały za intensyfikację wymiany ciepła, co zostało potwierdzone wyznaczonymi polami prędkości.

Manuscript received January 17, 2007; accepted for print May 28, 2007